Reexamination of the energy levels of ^{15}F by ^{14}O+^{1}H elastic resonance scattering

F. Q. Guo,[1,2] J. Powell,[1] D. W. Lee,[1,4] D. Leitner,[1] M. A. McMahan,[1] D. M. Moltz,[2] J. P. O'Neil,[3] K. Perajarvi,[1] L. Phair,[1] C. A. Ramsey,[3] X. J. Xu,[1] and Joseph Cerny[1,2]

[1]*Nuclear Science Division, Lawrence Berkeley National Laboratory, Berkeley, California 94720, USA*

[2]*Department of Chemistry, University of California, Berkeley, California 94720, USA*

[3]*Life Sciences Division, Lawrence Berkeley National Laboratory, Berkeley, California 94720, USA*

[4]*Department of Nuclear Engineering, University of California, Berkeley, California 94720, USA*

(Received 23 June 2005; published 30 September 2005)

The energy levels of ^{15}F have been measured by the $p(^{14}\mathrm{O},p)^{14}\mathrm{O}$ reaction. The 120 MeV ^{14}O radioactive ion beam was produced by the BEARS coupled cyclotron system at an intensity averaging 1×10^4 particles/second on target. Energy calibration was obtained using resonances from the $p(^{14}\mathrm{N},p)^{14}\mathrm{N}$ reaction. The two lowest resonances in ^{15}F were fitted with an R-matrix calculation. The fit to the ground state had $J^\pi = 1/2^+$ at 1.23 $\pm$ 0.05 MeV (width 0.5 $-$ 0.84 MeV), and the first excited state was $J^\pi = 5/2^+$ at 2.81 $\pm$ 0.02 MeV (width 0.30 $\pm$ 0.06 MeV), both relative to the mass-energy of the proton and ^{14}O. The ^{15}F ground state energy supports the disappearance of the $Z = 8$ proton magic number for odd Z, $T_z = -3/2$ nuclei.

DOI: 10.1103/PhysRevC.72.034312 PACS number(s): 27.20.+n, 25.40.Cm, 25.60.Bx, 21.10.Dr

I. INTRODUCTION

Light nuclei near and beyond the driplines provide a test bed for new nuclear structure phenomena, both from the experimental and the theoretical point of view [1]. In the past two decades, new phenomena such as halo nuclei [2–5], and the disappearance of magic number effects [6] along the neutron dripline (and the concomitant appearance of new magic numbers [7,8]), have been observed. It is of great interest to see the extent to which similar phenomena can be observed near the proton dripline. To explore these phenomena, it is essential to have accurate and detailed information on these exotic nuclei, i.e., their energy spectra, and the spins and parities of their levels. With the development of radioactive ion beams, it is possible to get information on nuclei far from the valley of stability that has been difficult or impossible to acquire by traditional methods.

Proton rich radioactive beams provided by BEARS (Berkeley Experiments with Accelerated Radioactive Species) [9,10] make it possible to explore light nuclei at or beyond the proton dripline. With the ^{14}O beam, the $T_z = -3/2$ nucleus ^{15}F has been investigated in inverse kinematics by elastic resonance scattering [11–13] of ^{14}O on a target containing hydrogen. ^{15}F has been of nuclear structure interest in a variety of calculations, including predictions of the energy levels of $T_z = -3/2$ nuclides [14,15] and the disappearance of magic number effects due to unbalanced neutron-proton ratios [16,17].

The magic numbers in the valley of stable isotopes reflect the shell closures [18]. As one moves toward and beyond the dripline, the "standard" magic numbers may disappear and new magic numbers may emerge [6,7,16,17]. A question has been raised about the possible disappearance of the proton shell closure around $Z = 8$ for $T_z = -3/2$ nuclides. The focus of this issue is the absolute position of the ground state of ^{15}F.

The energy levels of ^{15}F were investigated earlier by Kekelis *et al.* [19] and by Benenson *et al.* [20] with the low cross-section transfer reaction ^{20}Ne(^{3}He, ^{8}Li)^{15}F. Only two levels have been observed so far, the ground state and the first excited state. The energies adopted in 1991 for these two levels are 1.47 $\pm$ 0.13 and 2.77 $\pm$ 0.10 MeV, respectively, relative to the mass-energy of a proton and ^{14}O [21]; their widths are reported to be 1.0 $\pm$ 0.2 MeV and 0.24 $\pm$ 0.03 MeV, respectively. Since the cross section is small, about 1–4 μb, the statistics were poor for both states. Recently, these two levels have been reinvestigated by several authors [1,16,22] using two reactions: the elastic scattering reaction $^{14}\mathrm{O}+p\rightarrow{}^{15}\mathrm{F}$ and the transfer reaction $^{16}\mathrm{O}(^{14}\mathrm{N},^{15}\mathrm{C})^{15}\mathrm{F}$. While most of these experiments agree quite well with one another on the position of the first excited state, questions have remained about the energy and the width of the broad ground state. To clarify this issue, a new measurement of low-lying ^{15}F levels using elastic scattering of ^{14}O on a hydrogen target was completed and analyzed.

II. EXPERIMENT

The experiment was performed at the 88-Inch Cyclotron of the Lawrence Berkeley National Laboratory using a beam of ^{14}O produced by the BEARS system [9,10]. In BEARS, light radioactive isotopes are produced in small batches by the 10 MeV medical cyclotron at LBNL's Biomedical Isotopes Facility [23], then rapidly transported about 350 m via a helium-push gas transport line to the 88-Inch Cyclotron building. The radioactive gas takes the chemical form of carbon dioxide, which allows for cryogenic separation from the helium transport gas before injection into the 88-inch cyclotron's AECR-U ion source.

Oxygen-14 ($t_{1/2} = 71$ sec) is the second BEARS beam [after ^{11}C($t_{1/2} = 20$ min)], and it required considerable additional development, which is described in detail in Ref. [10]. In brief, ^{14}O was first produced in the form of $H_2{}^{14}O$ by bombarding a high-pressure gas target composed of nitrogen with a few percent hydrogen. The activated water vapor was separated from the unloaded target gas through momentary freezing at -40°C, and then chemically converted

to $[^{14}O]CO_2$ in two steps: $H_2{}^{14}O \rightarrow C\,{}^{14}O$ through reaction with graphite at 1000–1100°C, followed by oxidation over a platinum catalyst. Target unloading, water separation, and chemical conversion took about 15 s, after which the $[^{14}O]CO_2$ was rapidly transferred to the 88-Inch Cyclotron using the same BEARS systems developed for $^{11}CO_2$ [9]. One batch of activity consisted of 90 s of production and 15 s of loading and unloading. At the 88-Inch Cyclotron, the cryogenically separated $[^{14}O]CO_2$ was injected into the AECR-U ion source, using a variable valve to produce a steady gas flow.

As had been previously measured with ^{11}C beams [9], a significant slow component provided a long hold-up time in the AECR ion source. The beam of ^{14}O continued well after $[^{14}O]CO_2$ injection was finished. When corrected for the radioactive decay of ^{14}O, the beam intensity dropped with a half-life of about 3 min. This may reflect ^{14}O radicals sticking to the source walls, possibly with isotopic exchange effects. Unfortunately, though this effect is of little importance with the 20-min half-life of ^{11}C, with 71-s oxygen-14 it leads to large decay losses.

Oxygen-14 was extracted from the ion source in the 6+ charge state (which had the maximum yield) and accelerated to 120 MeV. Because the cyclotron cannot cleanly separate $^{14}O^{6+}$ from the much more intense $^{14}N^{6+}$, the beam was fully stripped to $^{14}O^{8+}$ by a thin foil and transported through two dipole magnets. However, it was found that the ^{14}O beam was still contaminated with lower energy $^{14}N^{7+}$of the same magnetic rigidity, presumably due to scattering from beamline components. Careful radiofrequency tuning was done to minimize this effect and obtain reasonable ^{14}O transmission efficiency while allowing less than 1% $^{14}N^{7+}$ contamination.

The final ^{14}O beam had an intensity that averaged about 10,000 pps on target, with a low of 8,000 and a maximum of about 30,000 pps. This is much lower than the maximum of 10^8 pps achieved with ^{11}C beams. Partially, this is due to the 20 times lower production yield of ^{14}O versus ^{11}C [24] as well as losses in the additional chemical processing steps. However, most the decrease is due to decay or isotopic exchange losses associated with the ion source.

The 120 MeV ^{14}O beam was directed onto a target consisting of a 17.8 μm nickel degrader followed by a thick (18.4 mg/cm^2) polyethylene foil. This target combination was chosen to completely stop 120 MeV ^{14}O (and ^{14}N, as a beam used for calibration).

Scattered protons from the polyethylene (PE) were observed in a ΔE-E silicon detector telescope at 0° in the lab (see Fig. 1). The ΔE and E detectors were 72 μm and 3 mm thick, respectively, and were at a distance of 14.6 cm from the target, subtending an angle of about ±5° in the lab frame (corresponding to ±10° about 180° in the center of mass). The beam intensity was occasionally measured by removing the thick target and counting the direct beam. Because of the variations (noted earlier) in the beam intensity, the total beam on target during runs could only be crudely estimated.

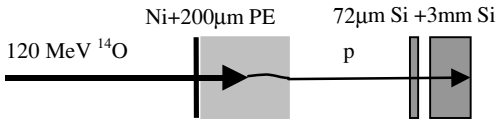

FIG. 1. The experimental setup for the $^{14}O+p$ thick target elastic resonance scattering experiment.

The advantage of this thick-target inverse-kinematics technique is simultaneous collection of the entire elastic-scattering excitation function, as the ^{14}O ions lose all their energy in the polyethylene target. The observed proton energies $E_{m,\mathrm{lab}}$ can be directly translated to the excitation energies of the reaction, $E_{\mathrm{c.m.}}$, by Eq. (1) [25]:

$$E_{\mathrm{c.m.}} = \frac{m+M}{4M\cos^2\theta_{\mathrm{lab}}} E_{m,\mathrm{lab}}. \quad (1)$$

A correction must be made to the observed proton energies due to energy losses in the target. Interactions at lower excitation energies occur deeper in the thick target thus reducing the amount of material remaining to retard the scattered proton. Thus, an energy loss correction factor can be calculated as a function of the center-of-mass energy, using knowledge of stopping powers, incoming beam energy, and target thicknesses. Stopping powers for ^{14}O, ^{14}N, and protons were calculated from SRIM [26].

To relate the observed yield of protons to a relative cross section versus energy, one must correct for the changing energy loss of the bombarding ion as it slows down [27]. The energy loss rate effectively determines the distance the ion travels into the target while in a specified energy interval, and thus the effective areal density of target protons. Thus yields must be multiplied by beam ion energy loss to calculate the elastic scattering excitation function:

$$\sigma \propto Y \times dE/dx. \quad (2)$$

The detector system was calibrated by using a beam of 120 MeV ^{14}N. Figure 2 shows the resulting spectrum of protons, which has been energy matched to previous experimental determinations of $^{14}N+p$ using conventional kinematics. The excitation functions from two such experiments are shown: lower energy measurements at $\theta_{\mathrm{c.m.}} = 168.1°$ from Olness *et al.* [28], and higher energy data at $\theta_{\mathrm{c.m.}} = 159.1°$ from West *et al.* [29]. A small nonlinear correction has been made at low energies for the calculated energy loss of the protons exiting the polyethylene target; otherwise the calibration is linear. The yield of protons in the thick-target inverse kinematics experiment has been corrected by the energy loss of ^{14}N in polyethylene [Eq. (2)] in order to produce a relative cross section.

The presence of several peaks and structures can be readily seen in the inverse kinematics data. These structures sit upon a significant background contributed by protons from ^{14}N reactions on the carbon component in the polyethylene target and on the nickel degrader foil. This background was investigated with a pure carbon target in place of the polyethylene target and was found to be featureless.

The experimental resolution can be determined from the width of the narrow resonance just below 3 MeV; it was found to be about 60 keV in the center of mass frame. The major contributions to this resolution were 40 keV from

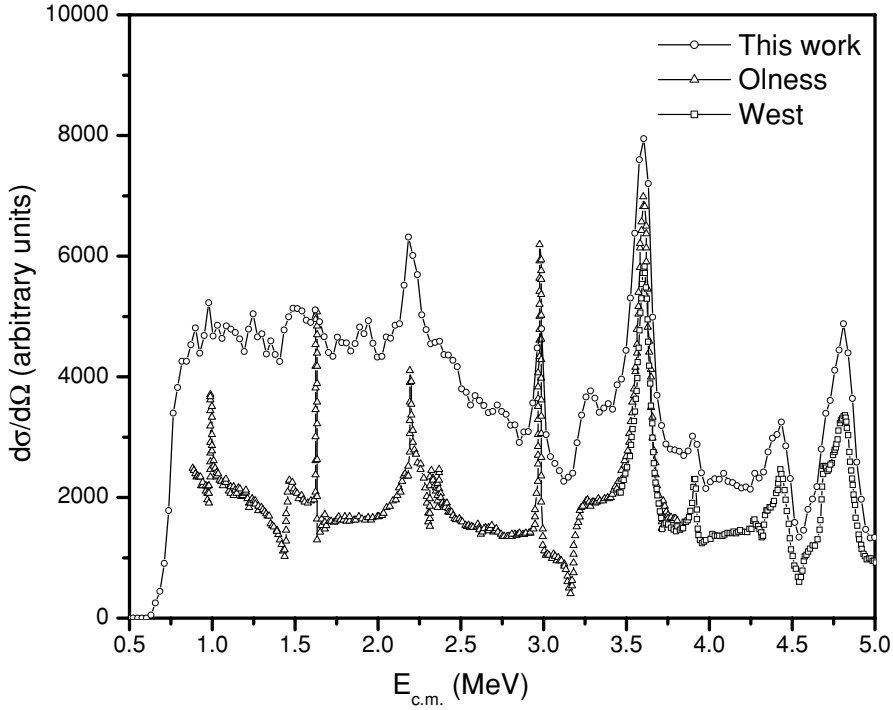

FIG. 2. The proton spectrum for the $p(^{14}\mathrm{N}, p)^{14}\mathrm{N}$ reaction. The upper line is from this experiment. The lower lines are from conventional kinematics: the lower energy data are from Olness *et al*. [28], and the higher energy data are from West *et al*. [29]. See text.

the E detector; 27 keV from the ΔE detector; 30 keV due to the $\pm 10^{\circ}$ angular spread in the center of mass; and 19 keV due to the beam spread and the straggling of both the incident beam and the scattering proton inside the degrader and target.

The features in the $^{14}\mathrm{N}+p$ spectrum permitted a good linear calibration of the detector telescope energy. This calibration was accurate to about 15 keV in the center of mass frame over the entire energy range from 1 to 5 MeV. However, a significant correction was required to use this calibration with $^{14}\mathrm{O}+p$. The more rapid energy loss of ^{14}O in the degrader foil and target lead to interactions occurring at a shallower depth, relative to the equivalent energy scattering by ^{14}N. Thus protons scattered by ^{14}O lose more energy as they emerge from the back of the target. The calculated energy loss corrections for ^{14}O and ^{14}N beams are displayed in Fig. 3.

It is important to know the accuracy of this calculation. SRIM [26], a Monte Carlo simulation program, has been used for the energy corrections. Since there are no direct experimental data for ^{14}N and ^{14}O ions with polyethylene, the experimental results of ^{16}O and ^{12}C with a polyethylene target [30] have been

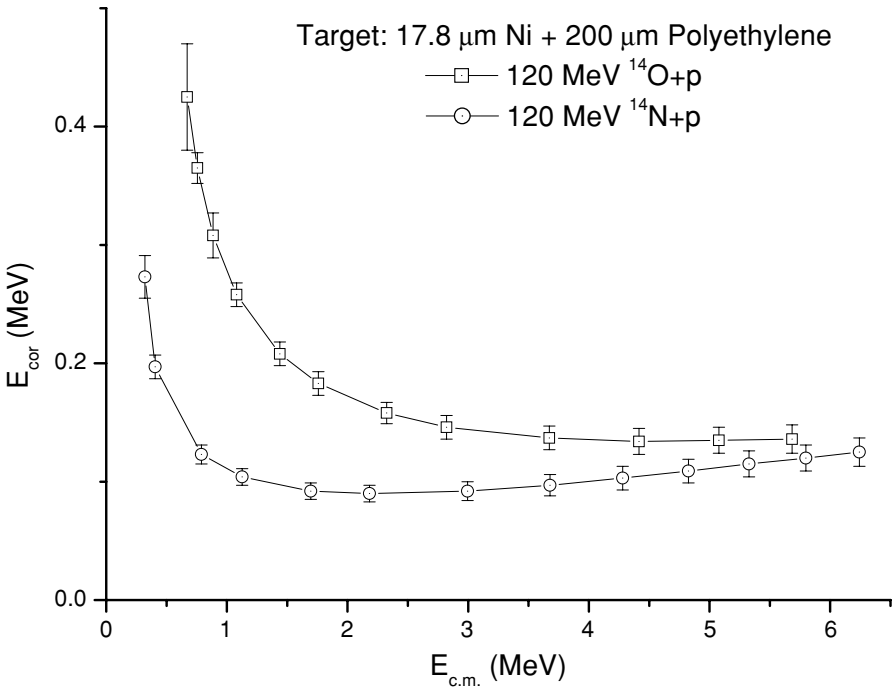

FIG. 3. The energy corrections for protons produced by two 120 MeV beams: ^{14}N and ^{14}O.

compared with the SRIM calculations. It is found that for ions with initial energy of about 10 MeV/nucleon, the calculation is about 6% less than the experimental data for both ^{16}O and ^{12}C when the energy is degraded to 1.5 MeV/nucleon. (A similar situation occurs for ^{40}Ar ions with polyethylene-like targets [31].) The interesting energy range in our experiment is about 1.5−8 MeV/nucleon. We have assumed the same behavior for ^{14}N and ^{14}O ions. Therefore, the systemic deviations in the experiment largely cancelled out when comparing ^{14}N and ^{14}O beams. The uncertainties for the final energy corrections are of the order of 15 keV in the center of mass.

III. *R*-MATRIX FORMALISM

The excitation function to be shown below is fitted with an *R*-matrix formalism [32]. The cross section, other than the Rutherford component, is expanded in terms of phase shifts for a spin 1/2 proton interacting with a spin zero particle, as described in Ref. [33]. The nuclear phase shift for each partial wave is taken to be equal to a hard sphere phase shift plus a possible resonant term that may contain one or more states:

$$\delta_\ell^\pm = -\phi_\ell + \arctan \frac{P_\ell R_\ell^\pm}{1-(S_\ell - b_\ell^\pm)R_\ell^\pm}, \tag{3}$$

where ϕ_ℓ refers to the hard sphere phase shift; δ_ℓ^+ and δ_ℓ^- refer, respectively, to the partial waves with proton spin aligned parallel or antiparallel to the orbital angular momentum, $\ell \cdot P_\ell$ and S_ℓ are the energy dependent *R*-matrix penetration and shift factors; $R_\ell^\pm$ is a sum over resonance terms $\gamma_\lambda^2/(E_\lambda - E)$ representing levels of that partial wave with reduced widths γ_λ^2; and $b_\ell^\pm$ is the *R*-matrix boundary constant. For cases where no more than one resonant term is required for each partial wave, the phase shift can be more clearly expressed as

$$\delta_\ell^\pm = -\phi_\ell + \arctan \frac{P_\ell \gamma_\lambda^2}{E_\lambda - E - (S_\ell - b_\ell^\pm)\gamma_\lambda^2}. \tag{4}$$

The formal *R*-matrix state parameters, E_λ and γ_λ^2, depend on the arbitrary boundary constant for that partial wave. Following standard convention, the boundary constant is set to be equal to the shift function at the state energy, $b_\ell^\pm = S_\ell(E_\lambda)$; with this choice, E_λ is defined as the "observed" resonance energy. To define an "observed" resonance width that is independent of energy, the penetration factor is approximated by its value at the state energy $P_\ell(E_\lambda)$, and the $S_\ell - S_\ell(E_\lambda)$ term is approximated by a series expansion about $E = E_\lambda$, keeping only the first non-zero term, $(E - E_\lambda)dS/dE|_{E=E_\ell}$, leading to

$$\delta_\ell^\pm \approx -\phi_\ell + \arctan \frac{\frac{1}{2}\Gamma_\gamma}{E_\lambda - E}, \tag{5}$$

where the "observed" width is defined as

$$\Gamma_\gamma = \left. \frac{2P_\ell \gamma_\gamma^2}{1+\lambda_\gamma^2 dS/dE} \right|_{E=E_\gamma}. \tag{6}$$

An additional important *R*-matrix parameter is the channel radius, which defines the "hard sphere" as well as the penetration and shift factors. We normally take this to be a simple estimate for ^{14}O+p: $1.25(A^{1/3}+1)$ with $A = 14$. However, it can also be varied as a free parameter.

IV. RESULTS

The results from two experimental runs utilizing 120 MeV ^{14}O on hydrogen are shown in Fig. 4. The yield from each run

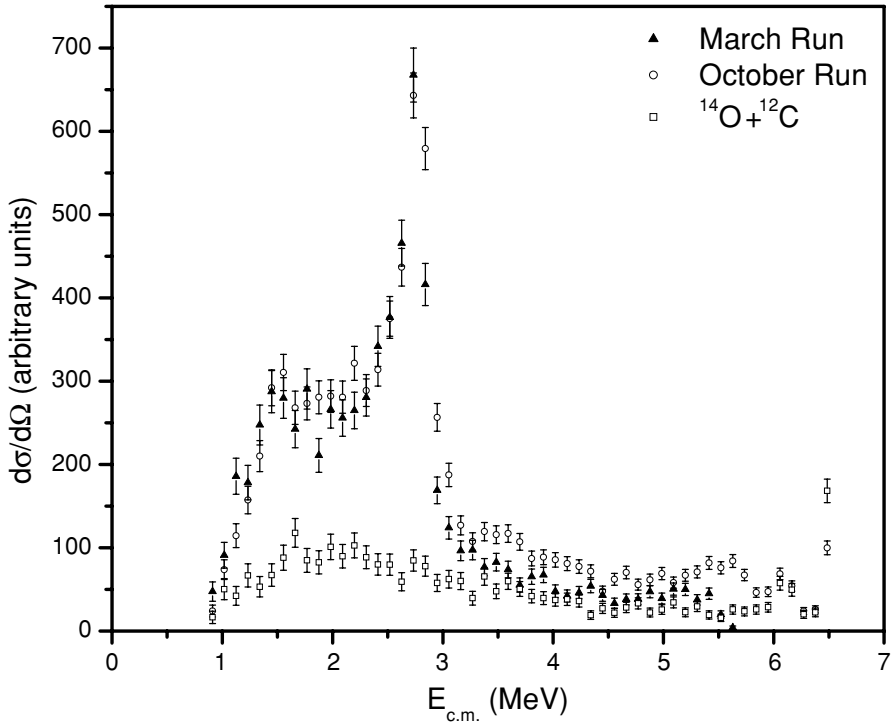

FIG. 4. The excitation functions for the two $p(^{14}\mathrm{O},p)^{14}\mathrm{O}$ runs. Also shown are the data for ^{14}O+^{12}C. The sharp "peak" around 6.5 MeV is due to an ADC overflow.

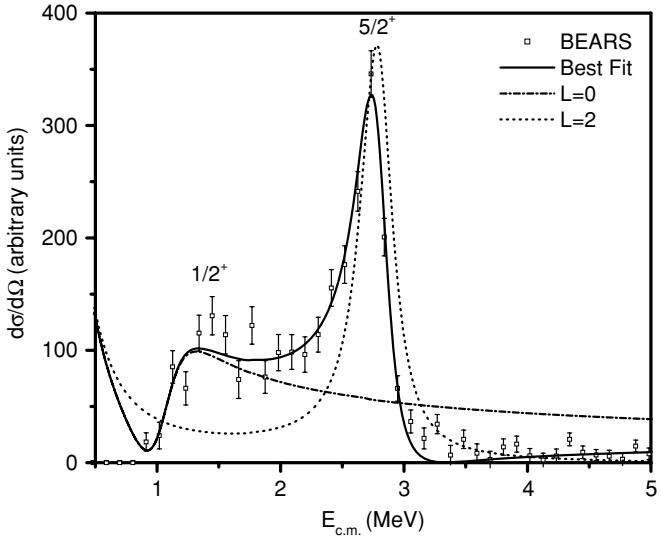

FIG. 5. The final ^{14}O+p excitation function and fitted curves.

has been multiplied by the energy loss of ^{14}O per unit thickness, dE/dx, in order to produce an excitation function. The first run in March 2003 was on a 17.8 μm nickel degrader and a 200 μm polyethylene target; the calibration of this run used the ^{14}N data of Fig. 2 as modified by a calculated correction for the different energy loss (see Fig. 3.)

The second run, (performed in October 2003), differed by having a thinner 14 μm nickel degrader. Unfortunately, detector and equipment problems prevented the determination of a good calibration spectrum for this run. Instead, the calibration was only determined by matching (with very poor statistics) to the two largest peaks in the ^{14}N+^{1}H spectrum, leading to an energy uncertainty of about 50 keV in the lower energy range. Despite this uncertainty, the shape of the spectrum from each of the two runs is very similar. The second

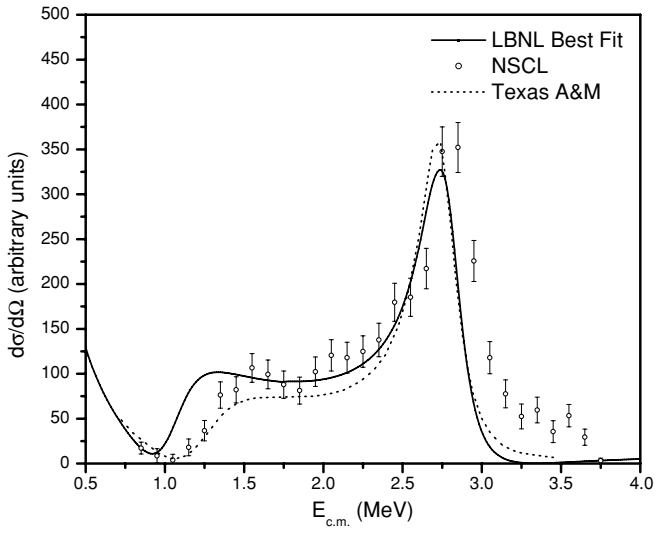

FIG. 6. The comparison of results from three different labs using the same $p(^{14}\mathrm{O},p)^{14}\mathrm{O}$ reaction.

TABLE I. The R-matrix parameters for ^{15}F from $p(^{14}\mathrm{O},p)^{14}\mathrm{O}$.

$E_{1/2+}$	1.23 ± 0.05 MeV
$\Gamma_{1/2+}$	$0.5 - 0.84$ MeV
$E_{5/2+}$	2.81 ± 0.02 MeV
$\Gamma_{5/2+}$ (observed)	0.30 ± 0.06 MeV

run also exhibits what appears to be a higher background at higher energies. This may reflect beam contaminants.

An ^{14}O+^{12}C background run is also shown in Fig. 4 for a 14 μm nickel degrader backed by a 28.0 mg/cm^2 carbon foil. This spectrum has been nominally energy calibrated and analyzed in the same way as the second ^{14}O+p run. The overall yield has been determinated using estimates of the ^{14}O beam intensity during these runs; this is accurate to only about 50%. The energy calibration should also include a different correction to account for the different target. However, since the background is a smooth featureless function, precise calibration is unnecessary.

Figure 5 shows an excitation function for elastically scattered protons on ^{14}O from the March run, which is preferentially used in the analysis because of its superior energy calibration. The background from ^{14}O+carbon has been subtracted from this ^{14}O+polyethylene run.

The ^{14}O+p scattering excitation function was fitted with two R-matrix resonances, a $1/2^+$ ground state ($\ell = 0$) and a $5/2^+$ first excited state ($\ell = 2$). This fit is shown in Fig. 5. Because of possible background at higher energies, the fit was made only between 1 MeV and 3.2 MeV. The fit has been convoluted with a nominal experimental resolution of 60 keV in the center of mass frame, though the exact resolution has little effect on the fit. Also shown are the separate contributions from each state, calculated by setting the reduced width of the other state to zero. Table I lists the best overall fit parameters. The minimum χ^2 was 27.9 (with 16 degrees of freedom).

The channel radius, used in defining the R-matrix hard sphere phase shift and penetration factors, was set equal to 4.26 fm, corresponding to $1.25(A^{1/3}+1)$ for ^{14}O+p. If allowed to be a free parameter, it was found to fit at 4.59 fm with a slightly better $\chi^2$of 26.8, and overall it lay within a range of roughly 3.5–5.5 fm. Variation in this range did not produce changes in the best fit parameters larger than the uncertainties given in Table I. Varying the angle used in the calculation, from $\theta_{\mathrm{c.m.}} = 180^\circ$ to 170°, the maximum angular range of the detector, also produced only small changes in the parameters.

Due to the uncertainty in the exact amount of ^{14}O+carbon background to subtract, this correction was varied by plus or minus 50% to investigate its effect on the best fit parameters. This is incorporated into the errors given in Table I, as are uncertainties in the energy calibration.

Other spin assignments were also investigated. The only one giving a possible, though poorer, fit was the assignment of the first excited state to be $3/2^+$, the other $\ell = 2$ possibility. This fit was notably worse than that with the preferred assignment of $5/2^+$, giving a best χ^2 of 39.2 versus 27.9. Reasonable fits could not be obtained with other choices of the angular momentum.

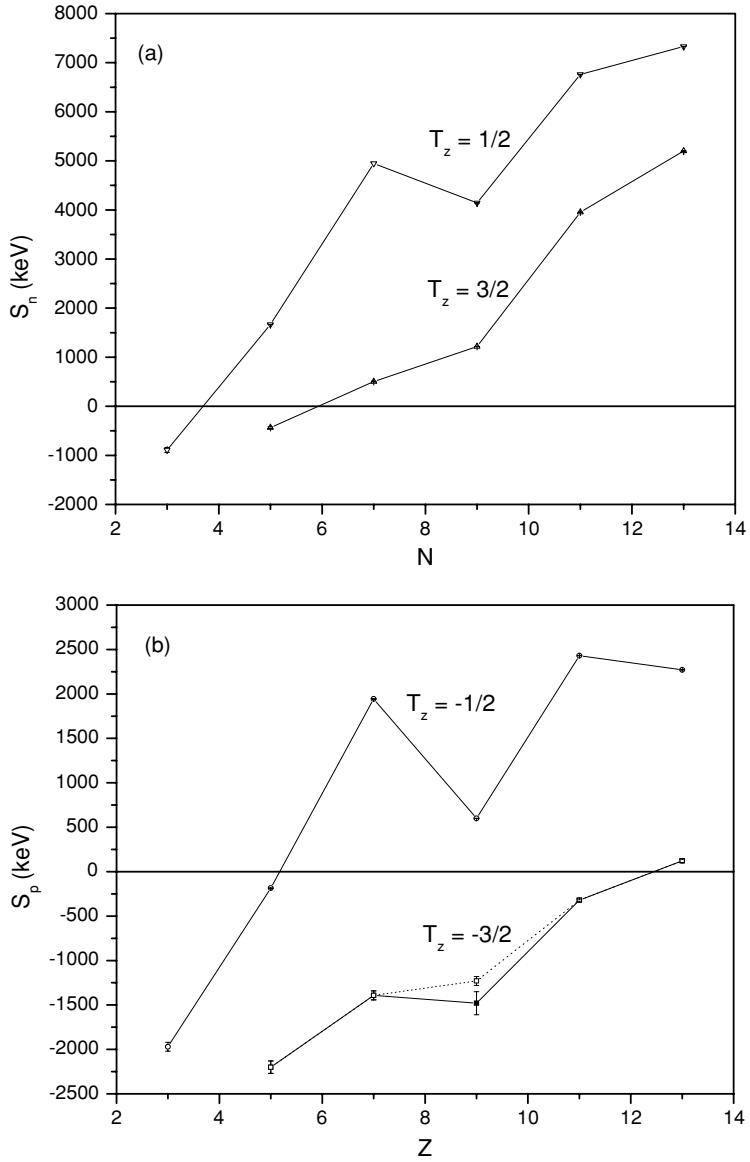

FIG. 7. Neutron and proton separation energies for different isospin series [15]. (a) S_n for $T_z = 1/2$ and $T_z = 3/2$ nuclei. (b) S_p for $T_z = -1/2$ and $T_z = -3/2$ nuclei.

The excitation function was measured to about 5 MeV, and there is no evidence of further resonances. However, the R-matrix calculations show that scattering from a ^{15}F mirror analog of the $1/2^-$ second excited state in ^{15}C at 3.103 MeV would have only a relatively small effect, and such a state could easily be hidden in the data. Better understanding and control of the background would be needed to identify or exclude such a state.

A comment should be made on the observed width of the broad $\ell = 0$ ground state. As seen from the definition of the observed width in Eq. (6), for large values of $\gamma_\lambda^2 dS/dE$, the observed width reaches a maximum of $2P_\ell(dS/dE)^{-1}$, independent of the reduced width. This limit is 0.84 MeV for the ground state. Near this limit, the behavior of the partial wave is determined mainly by the energy dependence of the penetration and shift functions, and by interference with the Rutherford scattering component. The best fit occurs at this limit, but reasonable fits are obtained for observed widths down to about 0.5 MeV.

V. DISCUSSION

These data can be compared with two other recent measurements of the ^{14}O+p spectrum.[1] Figure 6 displays the final excitation function of a NSCL group [16], as well as the fitted result for $\theta_{\text{c.m.}} = 180^\circ$ from a Texas A&M University group [22] (this fit is based on data from other angles, but it reasonably describes the 180° data in that work). Also plotted is the R-matrix fit from Fig. 5.

There is some disagreement among the three experiments. Our result agrees reasonably well with Ref. [22] as to the shape and position of the excited state, while showing systematic disagreements with the data of Ref. [16]. The current work disagrees with both previous measurements as to the position

[1]Comparisons to all prior past results for ^{15}F, which are complicated by the various possible definitions of the excitation energy and width of the broad states, are given in Ref. [13].

of the leading edge of the ground state resonance, placing this edge roughly 150 keV lower. This shift is larger than can be accounted for by the estimated energy uncertainties.

When experiments probe nuclei toward and beyond the driplines, the magic numbers may disappear and new magic numbers may emerge [6,7,16,17]. The systematics of neutron separation energies has been used to study the shell structure along the neutron dripline. There is evidence showing the disappearance of the $N = 8$ shell closure when close to the neutron dripline [16,17,34]. As shown in Figure 7(a) for $T_z = 1/2$ nuclei, shell closure is observed from the sharp drop between $N = 7$ and $N = 9$ nuclei in the plot of one neutron separation energies versus neutron number. However, there is no such drop for the $T_z = 3/2$ series, indicating the disappearance of the $N = 8$ shell.

Similarly, the systematics of proton separation energies can be used to study proton shell structure. It is arguable whether the disappearance of the $Z = 8$ shell closure happens when close to the proton dripline. Figure 7(b) shows proton separation energies for odd Z, even N nuclei with isospin $-1/2$ and $-3/2$. The shell closure in $T_z = -1/2$ nuclei can be clearly seen. Two different proton separation energies for ^{15}F are shown in this figure for the $T_z = -3/2$ nuclei: -1.23 MeV (dotted line) from this work and -1.48 MeV (solid line) from the most recent compilation [35]. For $T_z = -3/2$ nuclei, it depends on which S_p for ^{15}F is chosen, as to whether the (small) discontinuity vanishes. Our data would indicate the disappearance of the $Z = 8$ shell for proton-rich nuclei which are beyond the dripline.

VI. SUMMARY

Since the first successful delivery of ^{14}O as a radioactive ion beam at the 88-Inch Cyclotron, several $^{14}\mathrm{O}+p$ runs have been performed. Excellent energy calibration was obtained using the $^{14}\mathrm{N}+p$ reaction in inverse kinematics and comparing the results to those obtained in prior experiments with normal kinematics. The differences between $^{14}\mathrm{N}+^{1}\mathrm{H}$ and $^{14}\mathrm{O}+^{1}\mathrm{H}$ in the stopping power function have been evaluated for better energy calibration of the latter. After careful calibration, the energy levels of ^{15}F were fitted with an R-matrix calculation. Spins and parities were assigned to the two observed resonances. This new measurement of the ^{15}F ground state supports the disappearance of the $Z = 8$ proton magic number for odd Z, $T_z = -3/2$ nuclei.

ACKNOWLEDGMENTS

We thank the 88-Inch Cyclotron operations staff and Biomedical Isotope Facility staff for the beam development and the technical staff for their support in this experiment. This work was supported by the U.S. Department of Energy, Office of Nuclear Physics, under Contract No. DE-AC03-76SF00098 (Lawrence Berkeley National Laboratory).

[1] A. Lépine-Szily, J. M. Oliveira, D. Galante, G. Amadio, V. Vanin, R. Lichtenthäler, V. Guimarães, G. F. Lima, H. G. Bohlen, A. N. Ostrowski, A. Di Pietro, A. M. Laird, L. Maunoury, F. deOliveira Santos, P. Roussel-Chomaz, H. Savajols, W. Trinder, A. C. C. Villarid, and A. deVismes, Nucl. Phys. **A722**, 512 (2003).

[2] I. Tanihata, H. Hamagaki, O. Hashimoto, Y. Shida, and N. Yoshikawa, Phys. Rev. Lett. **55**, 2676 (1985).

[3] I. Tanihata, H. Hamagaki, O. Hashimoto, S. Nagamiya, Y. Shida, N. Yoshikawa, O. Yamakawa, K. Sugimoto, T. Kobayashi, D. E. Greiner, N. Takahashi, and Y. Nojiri, Phys. Lett. **B160**, 380 (1985).

[4] I. Tanihata, T. Kobayashi, O. Yamakawa, S. Shimoura, K. Ekuni, K. Sugimoto, N. Takahashi, T. Shimoda, and H. Sato, Phys. Lett. **B206**, 592 (1988).

[5] T. Kobayashi and O. Yamakawa, Phys. Rev. Lett. **60**, 2599 (1988).

[6] A. Navin, D. W. Anthony, T. Aumann, T. Baumann, D. Bazin, Y. Blumenfeld, B. A. Brown, T. Glasmacher, P. G. Hansen, R. W. Ibbotson, P. A. Lofy, V. Maddalena, K. Miller, T. Nakamura, B. V. Pritychenko, B. M. Sherrill, E. Spears, M. Steiner, J. A. Tostevin, J. Yurkon, and A. Wagner, Phys. Rev. Lett. **85**, 266 (2000).

[7] A. Ozawa, T. Kobayashi, T. Suzuki, K. Yoshida, and I. Tanihata, Phys. Rev. Lett. **84**, 5493 (2000).

[8] R. Kanungo, I. Tanihata, and A. Ozawa, Phys. Lett. **B528**, 58 (2002).

[9] J. Powell, R. Joosten, C. A. Donahue, R. F. Fairchild, J. Fujisawa, F. Q. Guo, P. E. Haustein, R.-M. Larimer, C. M. Lyneis, M. A. McMahan, D. M. Moltz, E. B. Norman, J. P. O'Neil, M. A. Ostas, M. W. Rowe, H. F. Van-Brocklin, D. Wutte, Z. Q. Xie, X. J. Xu, and J. Cerny, Nucl. Instrum. Methods Phys. Res. A **455**, 452 (2000).

[10] J. Powell, J. P. O'Neil, and J. Cerny, Nucl. Instrum. Methods Phys. Res. B **204**, 440 (2003).

[11] A. Galindo-Uribarri, J. Gomez del Campo, J. R. Beene, C. J. Gross, J. F. Liang, S. D. Paul, D. Shapira, D. W. Stracener, R. L. Varner, E. Chavez, A. Huerta, M. E. Ortiz, E. Padilla, and S. Pascual, Nucl. Instrum. Methods Phys. Res. B **172**, 647 (2000).

[12] K. Markenroth, Ph.D. thesis, Chalmers University of Technology and Göteborg University, Göteborg, Sweden, 2001.

[13] F. Q. Guo, Ph.D. thesis, University of California, Berkeley, California, 2004.

[14] M. S. Antony and J. Britz, Indian. J. Phys. A **62**, 411 (1988).

[15] J. Britz, At. Data Nuclear Data Tables **69**, 125 (1998).

[16] W. A. Peters, T. Baumann, D. Bazin, B. A. Brown, R. R. C. Clement, N. Frank, P. Heckman, B. A. Luther, F. Nunes, J. Seitz, A. Stolz, M. Thoennessen, and E. Tryggestad, Phys. Rev. C **68**, 034607 (2003).

[17] M. Thoennessen, AIP Conf. Proc. **680**, 293 (2003).

[18] K. S. Krane, *Introductory Nuclear Physics* (John Wiley and Sons, New York, 1987), p. 117.

[19] G. J. KeKelis, M. S. Zisman, D. K. Scott, R. Jahn, D. J. Vieira, J. Cerny, and F. Ajzenberg-Selove, Phys. Rev. C **17**, 1929 (1978).

[20] W. Benenson, E. Kashy, A. G. Ledebuhr, R. C. Pardo, R. G. H. Robertson, and L. W. Robinson, Phys. Rev. C **17**, 1939 (1978).

[21] F. Ajzenberg-Selove, Nucl. Phys. **A523**, 1 (1991).
[22] V. Z. Goldberg, G. G. Chubarian, G. Tabacaru, L. Trache, R. E. Tribble, A. Aprahamian, G. V. Rogachev, B. B. Skorodumov, and X. D. Tang, Phys. Rev. C **69**, 031302(R) (2004).
[23] H. F. VanBrocklin and J. P. O'Neil. in *Applications of Accelerators in Research and Industry*, edited by J. L. Duggan and I. L. Morgan (AIP Press, New York, 1997), pp. 1329–1332.
[24] S. W. Kitwanga, P. Leleux, P. Lipnik, and J. Vanhorenbeeck, Phys. Rev. C **42**, 748 (1990).
[25] K. Markenroth, L. Axelsson, S. Baxter, M. J. G. Borge, C. Donzaud, S. Fayans, H. O. U. Fynbo, V. Z. Goldberg, S. Grévy, D. Guillemaud-Mueller, B. Jonson, K.-M. Källman, S. Leenhardt, M. Lewitowicz, T. Lönnroth, P. Manngård, I. Martel, A. C. Mueller, I. Mukha, T. Nilsson6, G. Nyman, N. A. Orr, K. Riisager, G. V. Rogachev, M.-G. Saint-Laurent, I. N. Serikov, N. B. Shul'gina, O. Sorlin, M. Steiner, O. Tengblad, M. Thoennessen, E. Tryggestad, W. H. Trzaska, F. Wenander, J. S. Winfield, and R. Wolski, Phys. Rev. C **62**, 034308 (2000).
[26] J. F. Ziegler, The Stopping and Range of Ions in Matter (SRIM-2003), http://www.srim.org (2003).
[27] C. E. Rolfs and W. S. Rodney, *Cauldrons in the Cosmos* (University of Chicago Press, Chicago, 1988), pp. 289–310.
[28] J. W. Olness, J. Vorona, and H. W. Lewis, Phys. Rev. **112**, 475 (1958).
[29] M. L. West, C. M. Jones, J. K. Bair, and H. B. Willard, Phys. Rev. **179**, 1047 (1969).
[30] P. E. Schambra, A. M. Rauth, and L. C. Northcliffe, Phys. Rev. **120**, 1758 (1960).
[31] T. Alanko, J. Hyvonen, V. Kyllonen, P. Laitinen, A. Matilainen, J. Raisanen, and A. Virtanen, J. Phys. Condens. Matter **13**, 10777 (2001).
[32] A. M. Lane and R. G. Thomas, Rev. Mod. Phys. **30**, 257 (1958).
[33] R. A. Laubenstein and M. J. W. Laubenstein, Phys. Rev. **84**, 18 (1951).
[34] M. Thoennessen, RIKEN Review **39**, 68 (2001).
[35] G. Audi, A. H. Wapstra, and C. Thibault, Nucl. Phys. **A729**, 337 (2003).